Bioorganic Chemistry 86 (2019) 296–304

Contents lists available at ScienceDirect

Bioorganic Chemistry

journal homepage: www.elsevier.com/locate/bioorg

Tyrosinase and α-glucosidase inhibitory potential of compounds isolated from *Quercus coccifera* bark: *In vitro* and *in silico* perspectives

Suat Sari[a], Burak Barut[b], Arzu Özel[b,c], Ayşe Kuruüzüm-Uz[d], Didem Şöhretoğlu[d,*]

[a] Hacettepe University, Faculty of Pharmacy, Department of Pharmaceutical Chemistry, Sıhhiye, Ankara, TR-06100 Ankara, Turkey
[b] Karadeniz Technical University, Faculty of Pharmacy, Department of Biochemistry, Trabzon, Turkey
[c] Karadeniz Technical University, Drug and Pharmaceutical Technology Application and Research Center, Trabzon, Turkey
[d] Hacettepe University, Faculty of Pharmacy, Department of Pharmacognosy, Sıhhiye, Ankara, TR-06100 Ankara, Turkey

ARTICLE INFO

Keywords:
α-Glucosidase
Tyrosinase
Quercus
Polydatin
Molecular modelling

ABSTRACT

Bark of *Quercus coccifera* is widely used in folk medicine. We tested tyrosinase and α-glucosidase inhibitory effects of *Q. coccifera* bark extract and isolated compounds from it. The extract inhibited tyrosinase with an IC_{50} value of 75.13 ± 0.44 μg/mL. Among the isolated compounds, polydatin (**6**) showed potent tyrosinase inhibition compared to the positive control, kojic acid, with an IC_{50} value of 4.05 ± 0.30 μg/mL. The *Q. coccifera* extract also inhibited α-glucosidase significantly with an IC_{50} value of 3.26 ± 0.08 μg/mL. (-)-8-Chlorocatechin (**5**) was the most potent isolate, also more potent than the positive control, acarbose, with an IC_{50} value of 43.60 ± 0.67 μg/mL. According to the kinetic analysis, **6** was a noncompetitive and **5** was a competitive inhibitor of tyrosinase, and **5** was a noncompetitive α-glucosidase inhibitor. In the light of these findings, we performed *in silico* molecular docking studies for **5** and **6** with QM/MM optimizations to predict their tyrosinase inhibition mechanisms at molecular level and search for correlations with the *in vitro* results. We found that the ionized form of **5** (**5i**) showed higher affinity and more stable binding to tyrosinase catalytic site than its neutral form, while **6** bound to the predicted allosteric sites of the enzyme better than the catalytic site.

1. Introduction

Bark and young shoots of *Quercus coccifera* L. are used for the treatment of diabetes, diarrhea, and wounds in different parts of Anatolia [1–3]. Moreover, *Quercus* extracts applied for the treatment of hyperpigmentation in Persian Traditional Medicine [4]. The presence of tannins, flavonoids, and saponins in genus *Quercus* were reported before [5–7]. Some hydrolysable tannins were isolated from the leaves of *Q. coccifera*. Previously, we isolated two simple phenols, [kermesoside, (3-hydroxy-1-(4-hydroxy-3-methoxyphenyl)-propan-1-one) and 3-hydroxy-1-(4-hydroxy-3,5-dimethoxyphenyl)- propan-1-one], a megastigmane (cocciferoside), a tannin precursor [(-)-8-chlorocatechin], a stilbene derivative (polydatin), and two lignans (lyoniresinol-9-*O*-β-xylopyranoside and lyoniresinol-9-*O*-β-glucopyranoside) from bark of *Q. coccifera* [8].

Diabetes mellitus (DM) is a progressive degenerative disease characterized by abnormally high levels of glycemia. Diabetes dramatically increases the risk of cardiovascular problems, nephropathy, retinopathy, neuropathy, and some other neurodegenerative conditions like Alzheimer disease [9]. α-Glucosidase inhibitors are used for the treatment of type 2 DM. They affect carbohydrate digestion by inhibiting their conversion to monosaccharides thus limiting absorption by the intestines. Hence, α-glucosidase inhibitors reduce postprandial blood glucose and insulin levels [10].

The enzyme tyrosinase catalyzes the oxidation of simple phenols, which is the first step of the melanin biosynthetic pathway [11]. Melanin protects the skin from ultraviolet radiation but overproduction of melanin triggers several pigmentation disorders such as freckles, melanoma, and age spots in humans [12]. Tyrosinase also plays a key role in Parkinson's disease (PD) by converting dopamine to neuromelanin and its oxidation products, which are neurotoxic compounds associated with neurodegeneration in PD. Thus, it is important to limit tyrosinase to inhibit development of PD [13]. Furthermore, tyrosinase induces undesirable browning side effects in fruits and vegetables thereby cause loss of nutritional quality and value in the food industry [14]. Since tyrosinase inhibitors have potential applications in cosmetics, agriculture, and medicine, developing novel inhibitors with lower side effects is desirable [15].

In the present study, we tested α-glucosidase and tyrosinase inhibitory effects of the methanol extract from lower stems and bark of *Q.*

* Corresponding author.
E-mail address: didems@hacettepe.edu.tr (D. Şöhretoğlu).

https://doi.org/10.1016/j.bioorg.2019.02.015
Received 27 October 2018; Received in revised form 19 January 2019; Accepted 4 February 2019
Available online 05 February 2019
0045-2068/

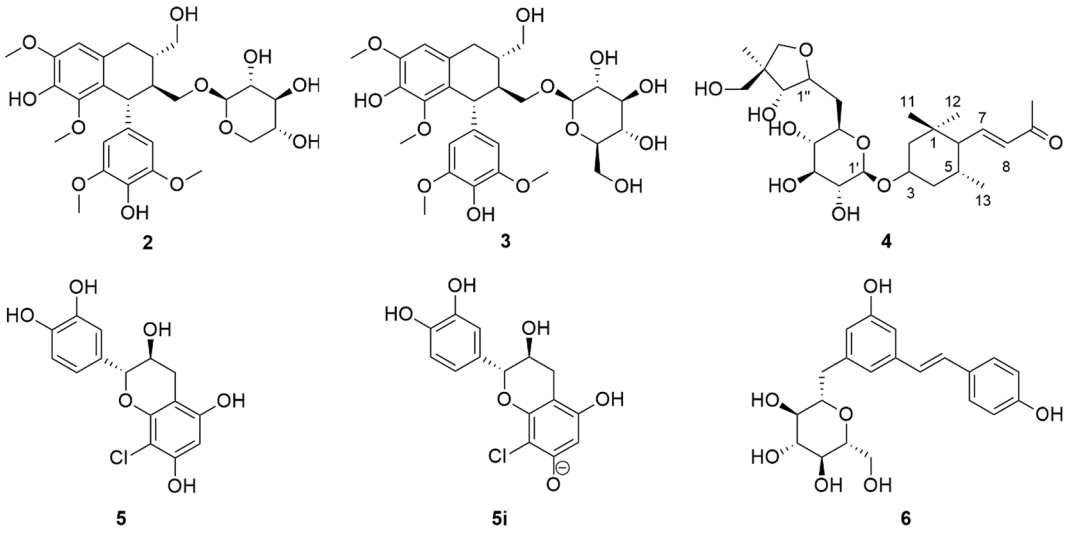

Fig. 1. Molecular structures of **2–6** and **5i.**

coccifera (1) as well as the isolated compounds [lyoniresinol-9-*O*-β-xylopyranoside (**2**) and lyoniresinol-9-*O*-β-glucopyranoside (**3**), cocciferoside (**4**), (-)-8-chlorocatechin (**5**), polydatin (**6**)] to find new hits (Fig. 1). We predicted druglikeness and pharmacokinetic properties of the active compounds *in silico*. We performed molecular docking studies in the catalytic and predicted allosteric ligand binding sites of mushroom tyrosinase to provide insights into tyrosinase inhibition mechanism of the active compounds.

2. Materials and methods

2.1. Materials and reagents

Q. coccifera L. was collected from Sertavul-Akçesme (Middle-South Anatolia, Turkey), in August 2008. A voucher specimen has been deposited in the Herbarium of the Faculty of Pharmacy, Hacettepe University, Ankara, Turkey (HUEF 10003). The tested compounds were isolated as previously described [8]. Trisma-base, L-3,4-dihydroxyphenylalanine (L-DOPA), kojic acid, tyrosinase from mushroom, methanol, acarbose, *p*-nitrophenyl-α-glucopyranoside (4-*p*NPG), and α-1,4-glucosidase (maltase) from *Saccharomyces cerevisiae* were obtained from Sigma-Aldrich (St. Louis, MO).

2.2. Enzyme inhibition assays

2.2.1. Tyrosinase inhibition

Tyrosinase inhibitory effects were assayed as described previously using L-DOPA as substrate [16]. Kojic acid was used as positive control. In order to examine the absorption maximum dopachrome at 475 nm, 100 μL of 0.1 M phosphate buffer pH 6.8, 20 μL of 250 U/mL tyrosinase, and extract/compounds at different concentrations were added into a microplate and incubated. Afterwards, 20 μL of 3 mM L-DOPA was pipetted to the solution and incubated for 15 min at room temperature. Then, the mixtures were measured using Multiskan™ Go microplate spectrophotometer at 475 nm. The inhibitory properties of extract/compounds against enzymes were expressed as the concentration that inhibited 50% of the enzyme activity (IC_{50}). IC_{50} values of the extract and the isolated compounds for tyrosinase were calculated using the Formula (1).

$$\% \text{ Inhibition} = (C - A)/C \times 100 \quad (1)$$

where C is the activity of the enzyme without extract or isolated compound and A is the activity of enzyme with extract or isolated compound.

2.2.2. α-Glucosidase inhibition

α-Glucosidase inhibitory properties of the extract and the compounds were monitored using a spectrophotometric method according to a previously reported method with slight modifications [17]. Acarbose was used as positive control. In brief, 100 μL of 0.5 U/mL α-glucosidase and the extract or the compounds at different concentrations were pipetted into a microplate and incubated for 15 min at room temperature. Afterwards, 50 μL of 5 mM 4-pNPG was added to the mixture. After incubation at room temperature for 15 min, the absorbance was measured at 405 nm using micro-plate spectrophotometer. IC_{50} values of the extract and the isolated compounds for α-glucosidase were calculated using the Formula (1).

2.2.3. Enzyme kinetics studies

In this work, Lineweaver-Burk and Dixon plots were used to investigate the kinetic parameters (inhibitor type and constant (K_i)) of **5** and **6** for tyrosinase and α-glucosidase [18–19]. For tyrosinase, the concentration of the enzyme was kept constant at 250 U/mL and various concentrations of L-DOPA (0.25–1.5 mg/mL) in the absence and presence of **5** and **6**. For α-glucosidase, the concentration of the enzyme was kept constant at 0.5 U/mL and different concentrations of 4-pNPG (0.25–1.5 mg/mL) in the absence and presence of **5**.

2.2.4. Statistical analysis

All the data was analyzed using GraphPad Prism 5.0. The results were expressed as mean ± standard deviation (n = 3). The differences among the compounds were investigated by unpaired *t* test. $p < 0.0001$ was considered to be significant.

2.3. Molecular modeling

2.3.1. Calculation of molecular descriptors and properties

In silico models of **5** and **6** were generated using MacroModel (2018-1: Schrödinger, LLC, NY, 2018) and optimized using OPLS_2005 force field parameters and conjugate gradient method [20,21]. A number of molecular descriptors and parameters relevant to physicochemical and pharmacokinetic properties were calculated using QikProp (2018-1: Schrödinger, LLC, NY, 2018). The results were compared with the reference values ranges derived from the experimental data of the known drugs and druglike molecules used to prepare QikProp.

2.3.2. Molecular docking

The crystal structure of mushroom tyrosinase with tropolone bound to the catalytic site (PDB ID: 2Y9X [22]) was downloaded from RCSB

Protein Data Bank (PDB) (www.rcsb.org) [23] and prepared using Protein Preparation Wizard of Maestro (2018–1: Schrödinger, LLC, NY, 2018). In this process ionization and tautomeric states were generated by Epik (2018-1: Schrödinger, LLC, New York, NY, 2018) and proton orientations were set by Propka. Grid maps of the receptor sites were prepared for docking using grid generation module of Maestro. For the catalytic site (site 1) the central coordinates of tropolone was taken as the centroid of the search space, for site 2–4 previously reported coordinates were used [16]. Molecular docking was performed using Glide (2018-1: Schrödinger, LLC, New York, NY, 2018) at standard precision mode with 50 runs for each ligand [24–26]. For AutoDock 4 (v4.2.6) and AutoDock Vina (v1.1.2), the ligands and the prepared protein were converted to the relevant format recognized by AutoDock [27,28]. Grid maps were prepared for each ligand using AutoGrid for AutoDock 4; this process is not required for AutoDock Vina. On AutoDock, each ligand was docked 50 times to the receptor using Lamarckian genetic algorithm at medium exhaustiveness. On AutoDock Vina, where docking operations are fully automated, the default settings were preferred. AutoDockTools was used for docking operations on AutoDock and AutoDock Vina. Using these software we redocked tropolone to the catalytic site and compared the results with its original conformation. All the software produced binding modes close to that of the co-crystallized ligand (RMSD: 1.33 Å for Glide, 2.00 Å for AutoDock, and AutoDock Vina 2.45 Å).

2.3.3. QM/MM calculations

For each selected **5**-2Y9X and **5i**-2Y9X complex obtained from Glide we performed QM/MM calculations using QSite (2018-1, Schrödinger, LLC, NY, 2018) and density functional theory (DFT). To define QM sites we picked the ligand for each complex. Force field minimization was applied to optimize QM regions with maximum 100 iterations using OPLS_2005 force field parameters.

3. Results and discussion

3.1. Inhibition of α-glucosidase, and tyrosinase

The inhibitory properties of the extract and the isolated compounds on tyrosinase were analyzed and their IC_{50} values were shown in Table 1. The IC_{50} value of the *Q. coccifera* extract was found to be 75.13 ± 0.44 μg/mL. Compound **6** had the highest inhibitory effect on tyrosinase with a 4.05 ± 0.30 μg/mL IC_{50} value. Kojic acid was used as positive control and its IC_{50} value was determined as 50.75 ± 0.25 μg/mL. The results indicated that **6** was approximately 12.5-fold more potent than kojic acid. Furthermore, **5** showed reasonable inhibition with an IC_{50} value of 60.24 ± 1.35 μg/mL.

The extract inhibited α-glucosidase significantly with an IC_{50} value of 3.26 ± 0.08 μg/mL. **5** had the highest α-glucosidase inhibitory effect among the isolated compounds and acarbose with an IC_{50} value of 43.60 ± 0.67 μg/mL. The IC_{50} values of **2** and **6** were above 1000 μg/mL, **3** and **4** were determined as 599.50 ± 8.04 and 561.75 ± 6.93 μg/mL, respectively. These compounds showed no or little inhibition compared to acarbose (IC_{50}: 50.45 ± 0.20 μg/mL) (Table 1).

Table 1
IC_{50} values (μg/mL) of the extract and the isolated compounds for tyrosinase and α-glucosidase.

Test material	Tyrosinase	α-Glucosidase
Extract	75.13 ± 0.44[a]	3.26 ± 0.08[a]
2	> 250	> 1000
3	> 250	599.50 ± 8.04[a]
4	> 250	561.75 ± 6.93[a]
5	60.24 ± 1.35[b]	43.60 ± 0.67[c]
6	4.05 ± 0.30[a]	> 1000
Acarbose	–	50.45 ± 0.20
Kojic acid	50.75 ± 0.25	–

[a] $P < 0.0001$.
[b] $P < 0.05$.
[c] Not significant compared to positive controls.

Table 2
Kinetic parameters of **5** and **6.**

	Tyrosinase		α-Glucosidase	
	Type	K_i (μg/mL)	Type	K_i (μg/mL)
5	Competitive	50.10 ± 0.20	Noncompetitive	30.05 ± 0.25
6	Noncompetitive	6.80 ± 0.10	–	–

The inhibition types and K_i values of **5** and **6** against tyrosinase and **5** for α-glucosidase were measured by using Lineweaver-Burk and Dixon plots. As shown in Table 2 and Fig. 2a, the K_m value of the enzyme for **5** increased without changing V_{max} indicating that **5** was a competitive inhibitor of tyrosinase. The competitive inhibitors show similar chemical structure to the substrate and compete with each other for binding to the catalytic site of the enzyme [29]. On the other hand, V_{max} value decreased in the presence of **6** and the substrate at increasing concentrations while K_m remained the same (Fig. 2c). This result indicated that **6** inhibited tyrosinase in noncompetitive manner, i.e. it binds to the enzyme and the enzyme-substrate complex. K_i values of **5** and **6** on tyrosinase were found to be 50.10 ± 0.20 and 6.80 ± 0.10 μg/mL, respectively (Table 2).

As shown in Fig. 3, the K_m value was fixed and the V_{max} value increased with increasing concentrations of **5**, showing that **5** was a noncompetitive inhibitor of α-glucosidase. K_i value of **5** for α-glucosidase was 30.05 ± 0.25 μg/mL.

There are some reports on tyrosinase inhibitor potential of *Quercus* species. 100 μg/mL 80% methanol extract of galls of *Q. infectoria* reportedly showed 59.3% tyrosinase inhibition in B16/F10 cells [4]. 133.33 μg/mL 80% ethanol extracts of raw, roasted and boiled acorns of *Q. coccifera* were showed to inhibit tyrosinase at 10.13%, 4.84%, and 2.95%, respectively. In the same study, 133.33 μg/mL positive control, kojic acid, inhibited tyrosinase at 83.97% [30]. Kim et al., isolated some polyamine derivatives from bee pollen extract of *Q. mongalica* and tested their effects on tyrosinase enzyme. Among them, a spermidine derivative containing three *trans*-coumaroyl units and another spermidine derivative containing two *cis*-coumaroyl and a *trans*-coumaroyl moieties exhibited higher tyrosinase inhibitory potential than the other isolated compounds. They indicated that compounds with coumaroyl moieties were more active than those with caffeoyl moieties [31]. In our study, we found the IC_{50} of **6** as 10.38 μM. It was consistent with the previously published value (14 μM) by Uesugi et al. **6** is a glucoside of resveratrol, a well-known and widely used phytochemical. Uesugi et al. also reported that tyrosinase inhibitory potential of **6** was stronger than that of resveratrol [32]. Moreover, recent studies highlighted that **6** may have higher bioavailability and possess better activity than resveratrol. Thus, **6** has attracted attention of researchers due to the possibility of being a good alternative for resveratrol regarding its bioavailability problem [33].

Ethanol extracts of two different batches of toasted wood of *Q. robur* reportedly inhibited α-glycosidase with IC_{50} values of 9.51 and 13.09 μg/mL. The major compound of the most active sub-fraction of these extracts was found to be a hydrolysable tannin, castalagin [34]. Moreover, catechin, epicatechin, and tiliroside isolated from *Q. gilva* leaves were reported to inhibited α-glycosidase with IC_{50} values of 168.60, 920.60, and 28.36 μM. Besides, tiliroside inhibited enzyme in an uncompetitive manner with a *Ki* value of 129.03 μM [35]. There is no report on α-glucosidase inhibitory effect of **5**. However, when we compared our result (IC_{50}: 150 μM) to that of catechin, it appeared that Cl substitution increased the inhibitory potential.

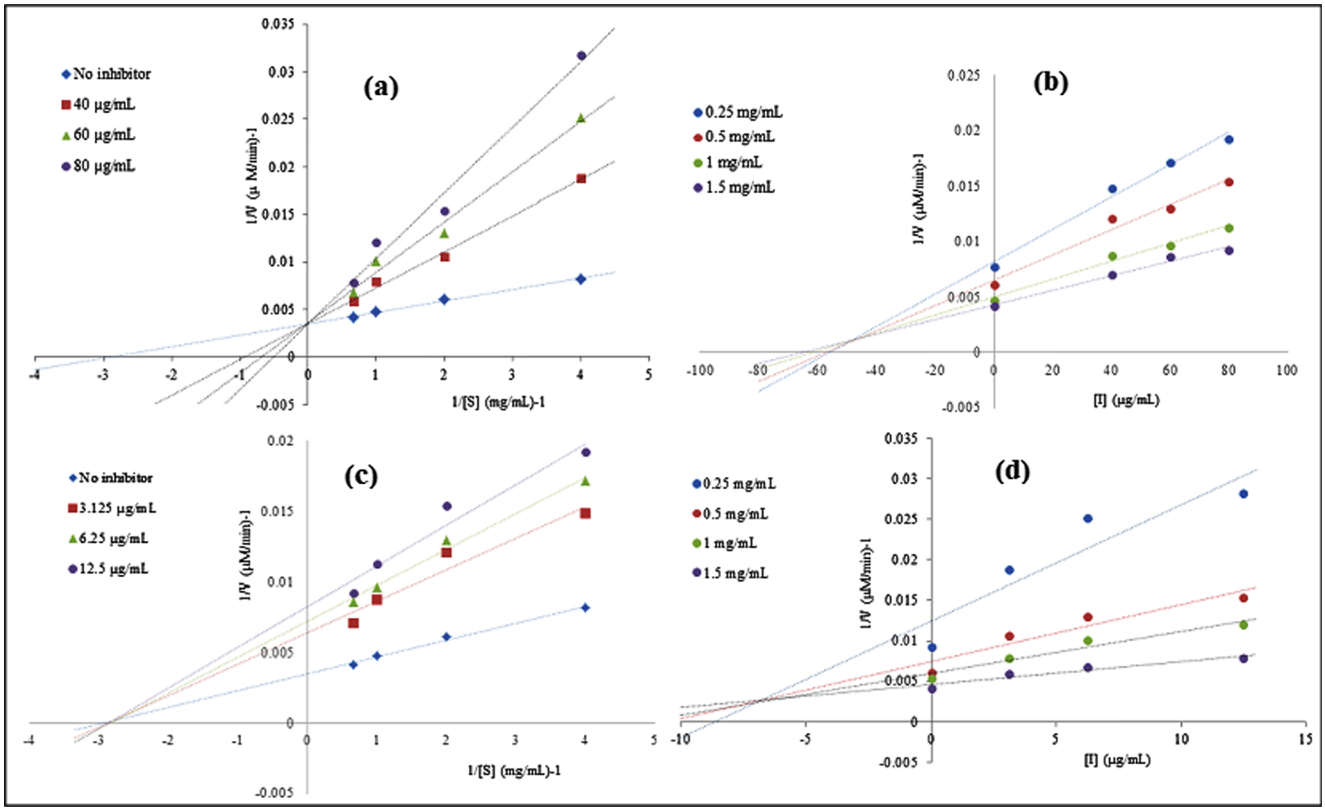

Fig. 2. Lineweaver-Burk and Dixon plots of **5** (a, b) and **6** (c, d) for tyrosinase.

3.2. Molecular modelling

For molecular modelling studies, we created and optimized 3D models of **5** and **6**. In the physiological conditions **5** occurs in neutral and ionized form (**5i**) (Fig. 1), therefore **5i** was included in all calculation and predictions along with **5**.

3.2.1. Prediction of druglikeness and pharmacokinetic properties

Poor physicochemical properties account for high attrition rates and cause loss of resources and time. Therefore, addressing physicochemical issues in the early stages of drug discovery is paramount [36]. We calculated a number of pharmaceutically relevant molecular descriptors and properties for the active compounds, **5** and **6**, some of which are presented in Table 3.

Among the properties and descriptors, molecular weight (MW), hydrogen donor and acceptor counts (donorHB and accptHB), octanol/water coefficient (QPlogPo/w), aqueous solubility (QPlogS), number of metabolic relations (#metab), and human serum albumin binding (QPlogKhsa) values were calculated within the ranges for druglike chemical space. On the other hand, the predicted IC_{50} for hERG inhibition was below the concerning limit for **6**. The predicted value of apparent permeability of Caco-2 cells, a model for the gut-blood barrier, was moderate for **5** and low for **6**. The same was true for the predicted apparent MDCK cell permeability values, a parameter for blood-brain barrier passage. The predicted brain/blood partition coefficient value of **6** was also below the limit. Thus, we can conclude that these compounds would have limited effects on the CNS. The compounds were also predicted to have moderate oral absorption. According to these results the compounds complied with the Lipinski's rule of five (RuleOfFive) (MW < 500, QPlogPo/w < 5, donorHB ≤ 5, accptHB ≤ 10) except **6**'s slightly high H bond acceptor value. They also fit to Jorgensen's rule of three (RuleOfThree) (QPlogS > -5.7, QP PCaco > 22 nm/s,

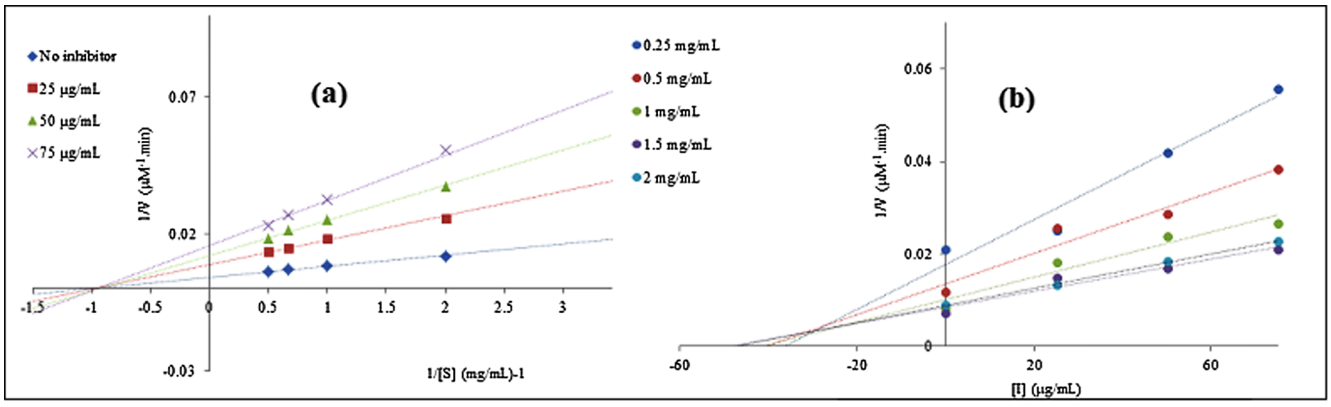

Fig. 3. Lineweaver-Burk and Dixon plots of **5** (a, b) against α-glucosidase.

Table 3
Some of the molecular descriptors/properties calculated for **5** and **6**.

Property or descriptor	Description	5	6	Range or recommended values
MW	Molecular weight (g/mol)	324.7	390.4	130.0–725.0
donorHB	Estimated number of hydrogen bonds that would be donated by the solute to water molecules in an aqueous solution	5	6	0.0–6.0
acceptHB	Estimated number of hydrogen bonds that would be accepted by the solute from water molecules in an aqueous solution	5.45	10.75	2.0–20.0
QPlogPo/w	Predicted octanol/water partition coefficient	0.93	0.14	–2.0 to 6.5
QPlogS	Predicted aqueous solubility, log S (S in mol dm^{-3})	−3.22	−2.98	–6.5 to 0.5
QPlogHERG	Predicted IC50 value for blockage of HERG K + channels	−4.79	−6.12	concern below –5
QPPCaco	Predicted apparent Caco-2 cell permeability (nm/sec.)	60.3	24.7	< 25 poor, > 500 great
QPlogBB	Predicted brain/blood partition coefficient	−1.74	−3.04	–3.0 to 1.2
QPPMDCK	Predicted apparent MDCK cell permeability (nm/sec.)	51.7	9.1	< 25 poor, > 500 great
#metab	Number of likely metabolic reactions	7	6	1–8
QPlogKhsa	Prediction of binding to human serum albumin.	−0.34	−0.75	–1.5 to 1.5
%HOA	Predicted human oral absorption on 0 to 100% scale	64.3	39.7	> 80% is high < 25% is poor
RuleOfFive	Number of violations of Lipinski's rule of five [37]	0	1	Compounds that satisfy these rules are considered druglike
RuleOfThree	Number of violations of Jorgensen's rule of three	1	0	Compounds with fewer violations of these rules are more likely to be orally available

Table 4
Docking scores (kcal/mol) of **5** and **5i** from Glide, AutoDock, and AutoDock Vina.

Ligand	Glide	AutoDock	AutoDock Vina
5	−5.7	−3.2	−5.1
5i	−5.6	−7.1	−5.9

#metab < 7) the number of **5**'s primary metabolites. The results for **5i** were the same as **5** for most cases and very close to **5** for the rest, therefore we did not include its results in Table 3.

3.2.2. *Tyrosinase inhibition: binding to the catalytic site*

The binuclear copper binding site of tyrosinase includes two Cu^{2+} ions each of which coordinates with imidazole N of three histidine

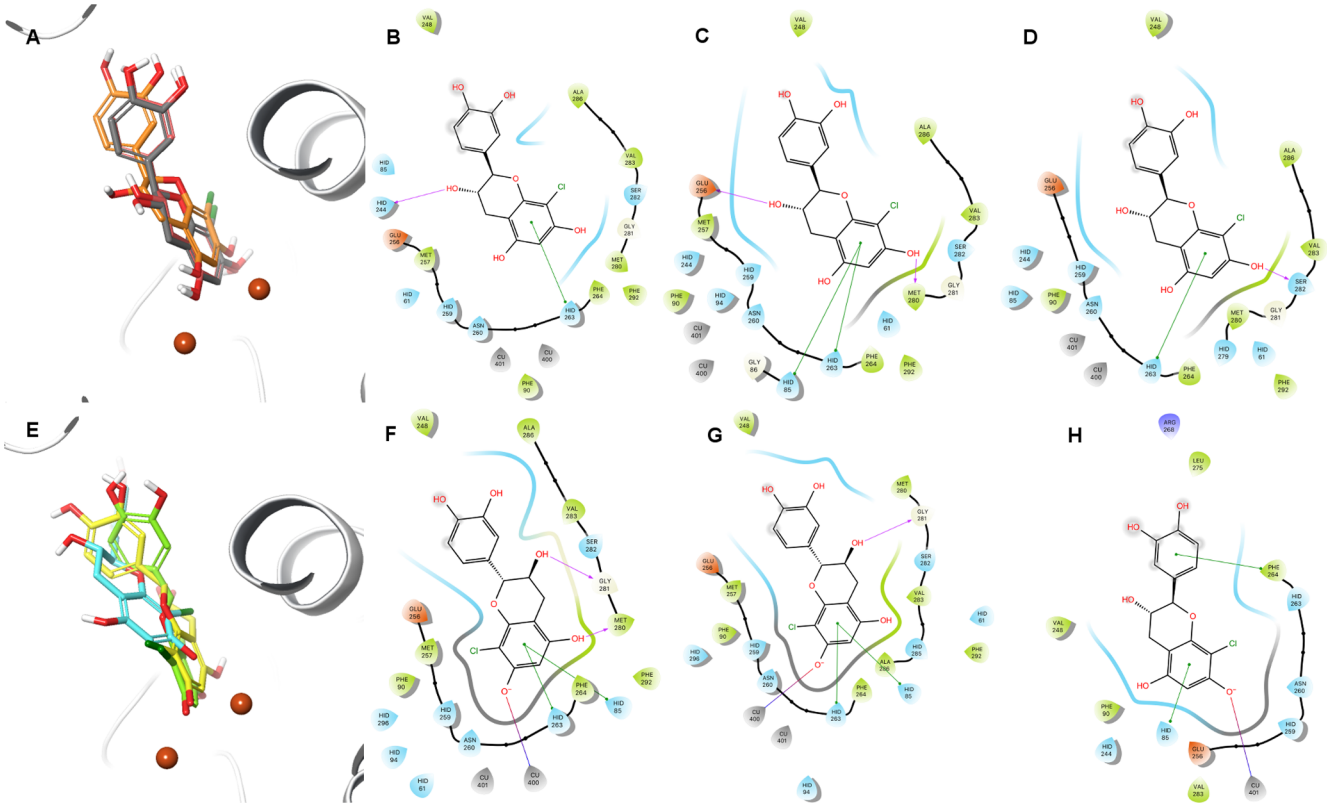

Fig. 4. Superposition of the binding poses of **5** (color sticks) from Glide (orange), AutoDock (gray), and AutoDock Vina (red) (A); 2D interaction diagrams of **5**-tyrosinase complexes from Glide (B), AutoDock (C), and AutoDock Vina (D); superposition of the binding poses of **5i** from Glide (yellow), AutoDock (green), and AutoDock Vina (cyan) (E); 2D interaction diagrams of **5i**-tyrosinase complexes from Glide (F), AutoDock (G), and AutoDock Vina (H); (For interpretation of the references to color in this figure legend, the reader is referred to the web version of this article.)

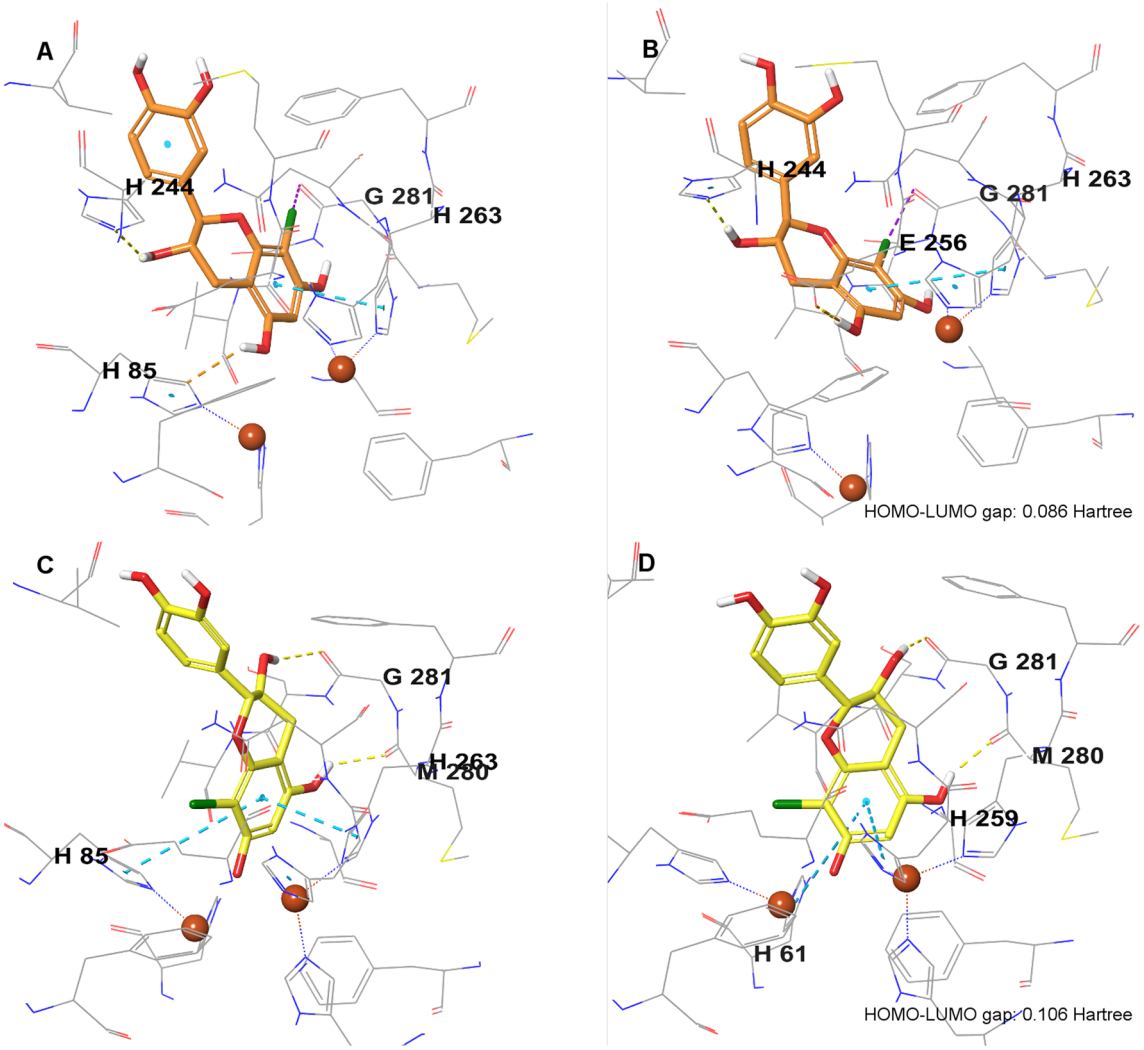

Fig. 5. The initial **5**-tyrosinase (A) and **5i**-tyrosinase (C) complexes obtained from Glide and the QM/MM optimized complexes (B and D). Residues within 4 Å of **5** (orange) and **5i** (yellow) are displayed. Protein residues are shown as color wireframe, Cu^{+2} as orange CPK, H bonds as yellow, π-π interaction as blue, and bad contacts as orange dashes. (For interpretation of the references to color in this figure legend, the reader is referred to the web version of this article.)

Table 5
Docking scores (kcal/mol) of **6** in site 1–4 of tyrosinase.

Site	Glide	AutoDock	AutoDock Vina
Site 1	−4.8	−3.3	−6.7
Site 2	−5.5	−4.1	−6.1
Site 3	−5.7	−4.7	−6.5
Site 4	−5.8	−4.5	−6.2

residues, which further interact with nearby residues to limit sidechain flexibility, hence support binding site stability. Therefore, in addition to direct interaction with the coppers, tyrosinase inhibitors display potent action by interacting with the copper ligands and the binding site residues connected to them [22].

5 bound to the tyrosinase catalytic site with similar affinity to **5i** according to Glide but with lower affinity according to AutoDock and AutoDock Vina (Table 4).

These two species differed more in the binding interactions with tyrosinase (Fig. 4). The hydroxyl oxygen at the 5th position of **5** interacted with both Cu^{2+} forming a triangle according to the results from three docking software. In the Glide's binding mode, **5** made a π-π interaction with His263, a copper ligand, and an H bond with His244, a binding site residue. In AutoDock's results, there was a π-π interaction with His85, another copper ligand, in addition to His263 and H bond with Glu256 and Met280, binding site residues, while AutoDock Vina produced a π-π interaction with His85 and an H bond with Ser282, another binding site residue. The three binding poses aligned well.

On the other hand, it was the O^{-} at the 7th position of **5i** which formed a triangle with the Cu^{2+} ions. This anion was slightly closer to one of the coppers to form a salt bridge. Glide and AutoDock predicted two π-π stacks, one with His85 and the other with His263, and an H bond with Gly281, another binding site residue. Glide also predicted another H bond with Met280. In the AutoDock Vina's results, there were two π-π stacks with His85 and Phe264, a binding site residue, as well. Glide's and AutoDock's binding poses for **5i** aligned well, AutoDock Vina's slightly tilted.

We performed QM/MM calculations for the **5**-tyrosinase and **5i**-tyrosinase complexes obtained from Glide to further optimize binding interactions and evaluate stability through HOMO and LUMO energies (Fig. 5). With molecular mechanics (MM) used in conventional docking methods, such as those we mentioned above, variations in electronic charges cannot be handled and accuracy of the predictions for ligand receptor interactions, especially those with metalloenzymes, may be compromised. Using quantum mechanics (QM) for the reactive sites of a ligand-receptor complex and treating the rest of the system with MM usually leads to accurate solutions within reasonable amount of time.

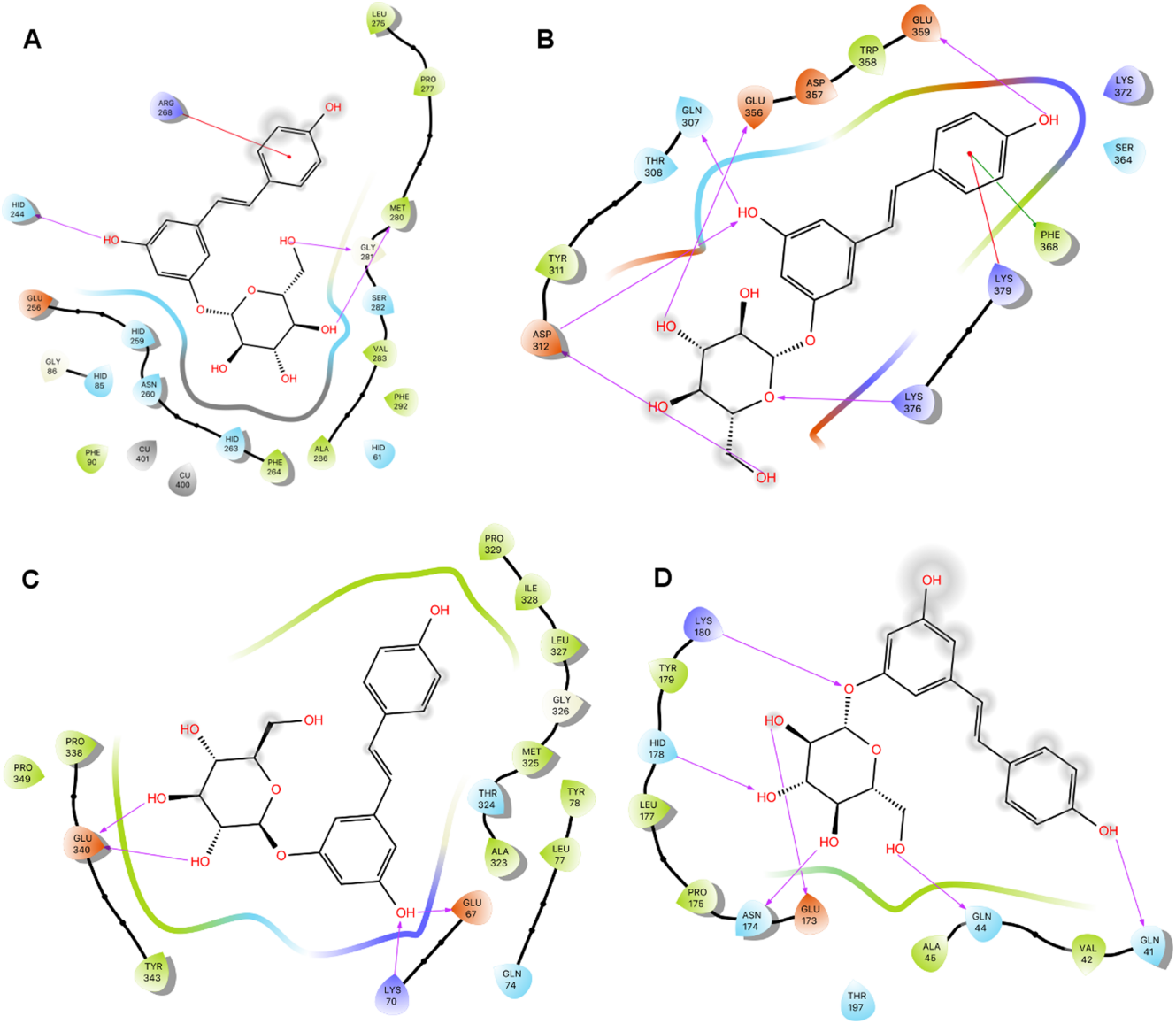

Fig. 6. 2D interaction diagrams of **6** with site 1–4 residues of tyrosinase.

In the QM/MM-optimized complex, **5** moved away from the Cu^{2+} region putting the hydroxyls at 3.11–3.37 Å away from one Cu^{2+} and much further from the other. The poor contact with His85 was replaced with a poor contact with Glu256. In the QM/MM-optimized binding of **5i**, which was more conserved than that of **5**, the π-π interactions with His85 and His263 shifted to His61 and His259, the latter two of which are also Cu^{2+} ligands. **5i** retained its position relative to the Cu^{2+} ions. The HOMO-LUMO gap, which indicates stability, was higher in the case of **5i**. These findings, along with forming salt bridge with Cu^{2+}, support the possibility of **5i**'s being a more potent tyrosinase inhibitor than its neutral form.

Generally, molecular modelling studies on the binding of **5** to tyrosinase catalytic site showed that the hydroxyl substitutions on the benzene of the 4-chromanone ring were responsible for interacting with Cu^{2+} ions, while this benzene alone conferred stability through interactions with Cu^{2+} ligands. In the case of **5i**, the O^- at the 7th position formed a salt bridge and the compound made a more stable complex with the enzyme than the neutral form.

In our previous study, we reported potent tyrosinase inhibitor flavonols, which have a benzene substitution (ring B) at the 2nd position of the chromone ring and hydroxyl substitutions on C-3′ and/or C-4′ of ring B [38]. These hydroxyl groups reportedly formed crucial H bond(s) with Glu322 hydroxylate, which was not possible in the case of **5** and **5i**, due to lack of aromaticity with their 4-chromanone ring. This caused the 4-chromanone ring to bend at the dihydropyranone portion and moved the hydroxyl group away from Glu322, which could be one of the reasons for lower IC_{50} of **5** compared to the previous flavonoids.

According to the calculations by Epik, the ionized form, **5i**, occurs at lower abundance at pH 7 ± 2. For example, **5** is present at 95% and **5i** at 5% at pH 7, while **5** is present at 63% and **5i** at 27% at pH 8. This could be another factor reducing **5**'s IC_{50} as **5i** was predicted to be the more potent form.

3.2.3. *Tyrosinase inhibition: binding to the allosteric sites*

Noncompetitive inhibitors are known to bind to regions other than substrate binding site of a given target macromolecule. In our previous study, we reported *in silico* identification and evaluation of three possible allosteric sites of mushroom tyrosinase [38]. We docked **6**, identified as a potent noncompetitive tyrosinase inhibitor, to the catalytic site (site 1) and the predicted allosteric sites (site 2–4) of tyrosinase to understand where and how **6** binds to tyrosinase. Docking scores from Glide and AutoDock showed that **6** preferred the allosteric sites, while

AutoDock Vina indicated the opposite (Table 5).

In the binding mode of **6** in site 1 obtained from Glide, the glucoside moiety reached to the Cu^{+2} region with hydroxyl oxygens roughly 3 Å away from each Cu^{2+} (Fig. 6). The conformationally restricted phenylethenylbenzene moiety of **6**, which was exposed to the solvent molecules, apparently prevented this sugar moiety to get closer to the Cu^{2+} ions. In site 2, the phenylethenylbenzene moiety of **6** fit in the deep cavity engaging in a number of π-π and H bonding interactions, while the sugar moiety faced the solvent, which was more viable than the binding pose in the catalytic site. In site 3, **6** engaged in H bonds and lipophilic interactions with the cavity residues both with phenylethenylbenzene and glucoside moieties, but the binding mode of **6** in site 4 was similar to site 1, i.e. the sugar moiety occupied the cavity with various H bonds and the phenylethenylbenzene was mostly exposed to the solvent. These findings indicated that **6** most probably bound to the allosteric sites, site 2 and site 3, of tyrosinase. Binding to multiple allosteric sites at the same time could account for **6**'s potent effect.

4. Conclusions

In this study, we tested tyrosinase and α-glucosidase inhibitory effects of an extract from the bark of *Q. coccifera* and the compounds isolated from it. Especially, the extract exhibited stronger α-glucosidase inhibitory activity with an IC_{50} value of 3.26 ± 0.08 μg/mL than acarbose (IC_{50}: 50.45 ± 0.20 μg/mL). Among the isolated compounds, **6** inhibited tyrosinase significantly, it was 12.5 fold more potent than kojic acid. Also, tyrosinase inhibitory effect of **5** was close to kojic acid. **5** was found to be a competitive tyrosinase inhibitor whereas **6** was an uncompetitive inhibitor. Further, **5** was determined as the most potent α-glucosidase inhibitor among the isolated compounds and more potent than acarbose with an IC_{50} 43.60 ± 0.67 μg/mL. According to the kinetic studies, **5** was a noncompetitive α-glucosidase inhibitor with K_i value of 30.05 ± 0.25 μg/mL. These results supports use of bark of *Q. coccifera* for the treatment of diabetes in folk medicine.

Upon predicting druglikenes and pharmacokinetic properties of **5** and **6** *in silico* we found that they mostly complied with the rules of druglike chemical space. The compounds were also predicted to have favorable pharmacokinetic properties despite a few exceptions. Molecular docking studies with multiple software and QM/MM approach showed that the **5** fit well to the catalytic site of tyrosinase and the 4-chromanone moiety with its hydroxyl groups was mainly responsible for the key interactions. The ionized form of **5** (5i) probably bound to this site tighter with better stability, especially with a better interaction profile with the Cu^{2+} ions. **6**, on the other hand, supposedly bound to the predicted allosteric sites rather than to the catalytic site, which was supported by the results from the enzyme kinetics study.

Appendix A. Supplementary material

Supplementary data to this article can be found online at https://doi.org/10.1016/j.bioorg.2019.02.015.

References

[1] G. Bulut, M.Z. Haznedaroğlu, A. Doğan, H. Koyu, E. Tuzlacı, An ethnobotanical study of medicinal plants in Acipayam (Denizli-Turkey), J. Herb. Med. 10 (2017) 64–81.

[2] S. Güneş, A. Savran, M.Y. Paksoy, M. Koşar, U. Çakılcıoğlu, Ethnopharmacological survey of medicinal plants in Karaisalı and its surrounding (Adana-Turkey), J. Herb. Med. 8 (2017) 68–75.

[3] E. Tuzlacı, Sifa niyetine, Türkiye' nin bitkisel halk ilaçları, Alfa Publishing, Istanbul, 2006.

[4] A. Jamshidzadeh, Y. Shokri, N. Ahmadi, N. Mohamadi, N. Sharififar, *Quercus infectoria* and *Terminalia chebula* decrease melanin content and tyrosinase activity in B16/F10 cell lines, J. Pharm. Pharmacogn. Res. 5 (2017) 270–277.

[5] M.K. Sakar, D. Söhretoglu, M. Özalp, M. Ekizoglu, S. Piacente, C. Pizza, Polyphenolic compounds and antimicrobial activity of *Quercus aucheri* Leaves, Turk. J. Chem. 29 (2005) 555–559.

[6] N. Fontana, G. Romussi, Triterpenoids, steroids and flavonoids from *Quercus virginiana*, Pharmazie 52 (1997) 331–332.

[7] H. Ito, K. Yamaguchi, T.H. Kim, S. Khennouf, K. Gharzouli, T. Yoshida, Dimeric and trimeric hydrolyzable tannins from *Quercus coccifera* and *Quercus suber*, J. Nat. Prod. 65 (2002) 339–345.

[8] D. Şöhretoğlu, A. Kuruüzüm-Uz, A. Simon, T. Patocs, M. Dekany, New secondary metabolites from *Quercus coccifera* L, Rec. Nat. Prod. 8 (2014) 323–329.

[9] D.M. Nathan, Long-term complications of diabetes mellitus, N. Engl. J. Med. 328 (1993) 1676–1685.

[10] H.S. Yee, N.T. Fong, A review of the safety and efficacy of acarbose in diabetes mellitus, Pharmacotherapy 16 (1996) 792–805.

[11] L. Zhang, X. Zhao, G. Tao, J. Chen, Z. Zheng, Investigating the inhibitory activity and mechanism differences between norartocarpetin and luteolin for tyrosinase: a combinatory kinetic study and computational simulation analysis, Food Chem. 223 (2017) 40–48.

[12] M. Fan, G. Zhang, X. Hu, X. Xu, D. Gong, Quercetin as a tyrosinase inhibitor: Inhibitory activity, conformational change and mechanism, Food Res. Int. 100 (2017) 226–233.

[13] Y. Xu, A. Stokes, W. Freeman, S.C. Kumer, B.A. Vogt, K.E. Vrana, Tyrosinase mRNA is expressed in human substantia nigra, Mol. Brain Res. 45 (1997) 159–162.

[14] L. Gou, J. Lee, H. Hao, Y. Park, Y. Zhan, Z. Lü, The effect of oxaloacetic acid on tyrosinase activity and structure: integration of inhibition kinetics with docking simulation, Int. J. Biol. Macromol. 101 (2017) 59–66.

[15] Y.-X. Si, S.J. Yin, S. Oh, Z.J. Wang, S. Ye, L. Yan, J.M. Yang, Y.D. Park, J. Lee, G.Y. Qian, An integrated study of tyrosinase inhibition by rutin: progress using a computational simulation, J. Biomol. Struct. Dyn. 29 (2012) 999–1012.

[16] D. Şöhretoğlu, S. Sari, B. Barut, A. Özel, Tyrosinase inhibition by a rare neolignan: inhibition kinetics and mechanistic insights through in vitro and in silico studies, Comput. Biol. Chem. 76 (2018) 61–66.

[17] D. Şöhretoğlu, S. Sari, A. Özel, B. Barut, α-Glucosidase inhibitory effect of *Potentilla astracanica* and someisoflavones: Inhibition kinetics and mechanistic insights through in vitro and in silico studies, Int. J. Biol. Macromol. 105 (2017) 1062–1070.

[18] H. Lineweaver, D. Burk, The determination of enzyme dissociation constants, J. Am. Soc. 56 (1934) 658–666.

[19] P. Butterworth, The use of Dixon plots to study enzyme inhibition, Biochim. Biophys. Acta (BBA) – Enzymol. 289 (1972) 251–253.

[20] L. Banks, H.S. Beard, Y. Cao, A.E. Cho, W. Damm, R. Farid, A.K. Felts, T.A. Halgren, D.T. Mainz, J.R. Maple, Integrated modeling program, applied chemical theory (IMPACT), J. Comput. Chem. 26 (2005) 1752–1780.

[21] E. Polak, G. Ribiere, Note sur la convergence de méthodes de directions conjuguées, R.I.R.O. 3 (16) (1969) 35–43, https://doi.org/10.1051/m2an/196903R100351.

[22] W.T. Ismaya, H.J. Rozeboom, A. Weijn, J.J. Mes, F. Fusetti, H.J. Wichers, B.W. Dijkstra, B.W. Crystal, Structure of agaricus bisporus mushroom tyrosinase: identity of the tetramer subunits and interaction with tropolone, Biochemistry 50 (2011) 5477.

[23] H.M. Berman, J. Westbrook, Z. Feng, G. Gilliland, T.N. Bhat, H. Weissig, I.N. Shindyalov, P.E. Bourne, The protein data bank, Nucl. Acids Res. 28 (2000) 235–242.

[24] R.A. Friesner, J.L. Banks, R.B. Murphy, T.A. Halgren, J.J. Klicic, D.T. Mainz, M.P. Repasky, E.H. Knoll, D.E. Shaw, M. Shelley, J.K. Perry, P. Francis, P.S. Shenkin, Glide: a new approach for rapid, accurate docking and scoring. 1. Method and assessment of docking accuracy, J. Med. Chem. 47 (2004) 1739–1749.

[25] R.A. Friesner, R.B. Murphy, M.P. Repasky, L.L. Frye, J.R. Greenwood, T.A. Halgren, P.C. Sanschagrin, D.T. Mainz, Extra precision glide: docking and scoring incorporating a model of hydrophobic enclosure for protein-ligand complexes, J. Med. Chem. 49 (2006) 6177–6196.

[26] T.A. Halgren, R.B. Murphy, R.A. Friesner, H.S. Beard, L.L. Frye, W.T. Pollard, J.L. Banks, Glide: a new approach for rapid, accurate docking and scoring. 2. Enrichment factors in database screening, J. Med. Chem. 47 (2004) 1750–1759.

[27] G.M. Morris, R. Huey, W. Lindstrom, M.F. Sanner, R.K. Belew, D.S. Goodsell, A.J. Olson, AutoDock4 and AutoDockTools4: automated docking with selective receptor flexibility, J. Comput. Chem. 30 (2009) 2785–2791, https://doi.org/10.1002/jcc.21256.

[28] O. Trott, A.J. Olson, AutoDock Vina: improving the speed and accuracy of docking with a new scoring function, efficient optimization, and multithreading, J. Comput. Chem. 31 (2010) 455–461, https://doi.org/10.1002/jcc.21334.

[29] E.N. Barut, B. Barut, S. Engin, S. Yildirim, A. Yaşar, S. Türkiş, A. Özel, F.S. Sezen, Antioxidant capacity, anti-acetylcholinesterase activity and inhibitory effect on lipid peroxidation in mice brain homogenate of *Achillea millefolium*, Turk. Biyokim. Derg. 42 (2017) 493–502.

[30] F.S. Şenol, N. Şekeroğlu, S. Gezici, E. Kılıç, İ. Erdoğan Orhan, Neuroprotective potential of the fruit (acorn) from *Quercus coccifera* L. Turk. J. Agric. For. 42 (2018) 82–87.

[31] S.B. Kim, Q. Liu, J.H. Ahn, Y.H. Jo, A. Turk, I.P. Hong, S.M. Han, B.Y. Hwang, M.K. Lee, Polyamine derivatives from the bee pollen of *Quercus mongolica* with tyrosinase inhibitory activity, Bioorg. Chem. 81 (2017) 127–133.

[32] D. Uesugi, H. Hamada, K. Shimoda, N. Kubota, S.I. Ozaki, N. Nagatani, Synthesis, oxygen radical absorbance capacity, and tyrosinase inhibitory activity of glycosides of resveratrol, pterostilbene, and pinostilbene, Biosci. Biotechnol. Biochem. 81 (2017) 226–230.

[33] D. Şöhretoğlu, M. Yüzbaşıoğlu Baran, R. Arroo, R.A. Kuruuzum-Uz, Recent advances in chemistry, therapeutic properties and sources of polydatin, Phytochem. Rev. (2018), https://doi.org/10.1016/j.compbiolchem.2018.06.003.

[34] V. Muccilli, N. Cardullo, C. Spatafora, V. Cunsolo, C. Tringali, α-Glucosidase inhibition and antioxidant activity of an oenological commercial tannin. Extraction, fractionation and analysis by HPLC/ESI-MS/MS and ^{1}H NMR, Food Chem. 215

(2017) 50–60.
[35] A.W. Indrianingsih, S. Tachibana, R.T. Dewi, K. Itoh, Antioxidant and α-glucosidase inhibitor activities of natural compounds isolated from *Quercus gilva* Blume leaves, Asian Pac. J. Trop. Biomed. 5 (2015) 748–755.
[36] M.J. Waring, J. Arrowsmith, A.R. Leach, P.D. Leeson, S. Mandrell, R.M. Owen, G. Pairaudeau, W.D. Pennie, S.D. Pickett, J. Wang, O. Wallace, A. Weir, An analysis of the attrition of drug candidates from four major pharmaceutical companies, Nat. Rev. Drug Discov. 14 (2015) 475–486.
[37] C.A. Lipinski, F. Lombardo, B.W. Dominy, P.J. Feeney, Experimental and computational approaches to estimate solubility and permeability in drug discovery and development settings, Adv. Drug Deliv. Rev. 46 (2001) 3–26.
[38] D. Şöhretoğlu, S. Sari, B. Barut, A. Özel, Tyrosinase inhibition by some flavonoids: inhibitory activity, mechanism by in vitro and in silico studies, Bioorg. Chem. 81 (2018) 168–174, https://doi.org/10.1016/j.bioorg.2018.08.020.